PROCEEDINGS OF SCIENCE

An Augmented QCD Phase Portrait: Mapping Quark-Hadron Deconfinement for Hot, Dense, Rotating Matter under Magnetic Field

Gaurav Mukherjee,[a,b,*] **D.Dutta**[a,b] **and D.K.Mishra**[a,b]

[a] *Bhabha Atomic Research Center, Mumbai 400085, India*

[b] *Homi Bhabha National Institute, Anushaktinagar, Mumbai 400094, India*

E-mail: phy.res.gaurav.m@gmail.com

QCD matter under extreme conditions prevailed in the microseconds-old universe and is created in ultra-relativistic heavy-ion collisions. In a generic non-central high-energy nucleus-nucleus collision the overlap region becomes a fireball of quark-gluon plasma (QGP) that sustains strong vorticity due to the finite impact parameter arising from the geometry of the collision and the resultant deposition of angular momentum. This QGP droplet may also be embedded in very powerful magnetic fields sourced initially by the spectator protons of the colliding nuclei and likely sustained or reinforced due to the conductivity and swirling charges of the QGP medium. This motivates the extension of the conventional T–μ_B planar phase diagram for QCD matter by augmenting it into a multi-dimensional domain spanned by temperature T, baryon chemical potential μ_B, external magnetic field B and angular velocity ω. Using two independent routes, one from a rapid rise in scaled entropy density and another dealing with a dip in the squared speed of sound, we identify the confinement-deconfinement transition in the framework of a modified statistical hadronization model. We find that this approach yields an estimate of the deconfinement temperature $T_C(\mu_B,\ \omega,\ eB)$ that is found to decrease with increasing μ_B, ω and eB with the most prominent drop (by nearly 40 to 50 MeV) in T_C occurring when all the three quasi-control (dependent on collision energy, centrality class, etc.) parameters are tuned simultaneously to finite values that are achievable in present and upcoming heavy-ion colliders. Potentially important magneto-rotational consequences on quark-hadron phenomenology are outlined including a proposal to reinterpret freeze-out data from peripheral collisions and use this as a 'magnetometer' and 'anemometer' probe.

42nd International Conference on High Energy Physics (ICHEP2024)
18-24 July 2024
Prague, Czech Republic

*Speaker

PoS(ICHEP2024)627

1. Motivation and introduction

The early universe and ultra-relativistic heavy-ion collisions (HIC) are arenas where the confined and deconfined phases of hot QCD matter dominate. In a typical non-central or peripheral high-energy nucleus-nucleus collision a fireball of quark-gluon plasma (QGP) forms. It may sustain swirling motion or vorticity (experiments [1] indicate $\omega \approx (9 \pm 1) \times 10^{21} s^{-1} \sim 0.006$ GeV, higher theoretical estimates [2] yield $\omega \sim 0.1$ fm$^{-1} \sim 0.02$ GeV) due to the finite impact parameter. This QGP droplet may also be embedded in very powerful magnetic fields ($eB \sim 0.12$ GeV^2) sourced initially by the spectator protons of the colliding nuclei [3] and likely sustained or reinforced due to the conductivity and swirling charges of the QGP medium [4]. This system, around 10 fm across and living for $\sim 10^{-23}$ s, is likely the hottest, densest, most vortical and embedded in the strongest known magnetic fields, albeit extremely briefly.

This motivates a suitable extension of the conventional (T–μ_B) planar phase diagram for QCD by augmenting it into a multi-dimensional domain spanned by temperature (T), baryon chemical potential (μ_B), external magnetic field (eB) and angular velocity (ω). Certain effects of finite μ_B, ω and eB, have been studied either separately or pairwise in the literature [5–8]. We explore their interplay and combined impact here. A detailed account can be found in our recently published paper [9].

We shall adopt a modified hadron resonance gas (HRG) model. Our investigation of the deconfinement (crossover) zone in the augmented QCD phase diagram should be relevant for present (RHIC, LHC) and upcoming (NICA, FAIR) colliders. Two independent methods of estimating the pseudo-critical temperature will be employed and shown to mutually corroborate. We conclude with some interesting implications of our findings and an outlook of future research.

2. Model formalism

We study a relativistic quantum ideal gas rigidly rotating and immersed in a uniform parallel magnetic field within a cylinder of radius R. In such a system composed of both charged as well as neutral particles the former couple with the background magnetic field while the latter do not, to a first approximation. To discuss just the magnetic coupling of a charged particle of charge Q, we need Landau levels, $\varepsilon = \sqrt{p_z^2 + p_\perp^2 + m^2} = \sqrt{p_z^2 + |QB|(2n + 1 - 2s_z) + m^2}$, with $n = 0, 1, 2, ...$ They appear in a finite-sized system with degeneracy $N = \frac{|QB|S}{2\pi}$ where $S \sim R^2$ ($S = \pi R^2$, for our geometry) is the transverse area. Landau quantization dominates as long as $N \gg 1$ or equivalently $\frac{1}{\sqrt{|QB|}} \ll R$. In words, the magnetic length ($\frac{1}{\sqrt{|QB|}} \equiv l_B$) which is the characteristic length scale for the cyclotron orbits, should be sufficiently smaller than the system size ($R = l_{\text{system}}$). The boundary or finite size become important when $l_{\text{system}} \lesssim l_B$ and the degenerate Landau quantized spectra no longer apply.

Since we use the Landau quantized levels we can investigate magnetic fields that are not too weak. The introduction of rigid rotation means the system must have a finite transverse size so that all speeds are below the vacuum speed of light, $c = 1$. This causality bound and Landau quantization together imply

$$1/\sqrt{|QB|} \ll R \leqslant 1/\omega. \tag{1}$$

The free energy density of the entire system in our model is the sum of the contributions from all the non-interacting hadrons and resonances in the HRG model. Our sought modifications to the standard HRG model, adapted to the scenario incorporating a uniform external magnetic field as well as a parallel rigid rotation have been deduced [6, 9, 10]. The free energy density for charged baryons and mesons is expressed as

$$f_{i,c}^{b/m} = \mp\frac{T}{\pi R^2}\int\frac{dp_z}{2\pi}\sum_{n=0}^{\infty}\sum_{l=-n}^{N-n}\sum_{s_z=-s}^{s}\ln(1\pm e^{-\frac{E_{i,c}}{T}}), \tag{2}$$

while that of the neutral ones [7, 9] is given by

$$f_{i,n}^{b/m} = \mp\frac{T}{8\pi^2}\int dp_r^2\int dp_z\sum_{l=-\infty}^{\infty}\sum_{\nu=l}^{l+2S_i}J_\nu^2(p_r r)\times\ln(1\pm e^{-\frac{E_{i,n}}{T}}), \tag{3}$$

where the dispersion relations provide the required energy spectra given by the rotation-modified levels (Landau levels for non-zero magnetic field):

$$E_{i,c} = \sqrt{p_z^2+m_i^2+|e_iB|(2n-2s_z+1)} \quad +\frac{e_i}{|e_i|}\omega(l+s_z)-\mu_i, \tag{4}$$

$$E_{i,n} = \sqrt{p_r^2+p_z^2+m_i^2}-(l+S_i)\omega-\mu_i. \tag{5}$$

Here e_i, S_i and m_i are the charge, spin and mass of the i^{th} hadron and the subscripts c and n refer to charged particles and neutral particles respectively. The chemical potential $\mu = Q_B\mu_B + Q_e\mu_e + Q_S\mu_S$ reflects the baryonic, electric charge and strangeness components. The upper (lower) signs correspond to the baryons (mesons) as denoted by the superscript b (m). The rotation is seen to alter the energy dispersion by an offset that effectively acts as a 'rotational' chemical potential by analogy [10]. We have taken fixed values of $r = 3$ GeV^{-1} and $R = 12.5$ GeV^{-1} (or $R = 2.5$ fm, $\sim$ typical system radius for peripheral collisions).

For the system we are dealing with, the free energy density reads $f = \epsilon - Ts - \mu_B n_B - \omega j - Bm_B = -p$, where pressure p, energy density ϵ, entropy density s, number density n_B, magnetization m_B and total angular momentum j are the relevant observables. All the observables here satisfy simple differential relations, $s = -\frac{\partial f}{\partial T}$, $n_B = -\frac{\partial f}{\partial \mu_B}$, $j = -\frac{\partial f}{\partial \omega}$, $m_B = -\frac{\partial f}{\partial B}$. The squared speed of sound is defined as $c_s^2 = \frac{\partial p}{\partial \epsilon}|_{(\mu_B,\omega,eB)} = [\frac{\partial p}{\partial T}|_{(\mu_B,\omega,eB)}]/[\frac{\partial \epsilon}{\partial T}|_{(\mu_B,\omega,eB)}]$ and here comes out to be

$$c_s^2 = \frac{s}{\left(T\frac{\partial s}{\partial T}+B\frac{\partial m_B}{\partial T}+\omega\frac{\partial j}{\partial T}+\mu_B\frac{\partial n_B}{\partial T}\right)\Big|_{(\mu_B,\omega,eB)}} \tag{6}$$

All hadrons, up to a mass of 1.5 GeV and excluding those having spin-3/2, listed in the particle data group list of particles contained in the package of THERMUS-V3.0 [12] have been included in our HRG model treatment. The ultraviolet mass cut-off is taken to reduce numerical cost and the exclusion of the spin-3/2 sector has been implemented due an instability in its theory [11].

3. An augmented phase diagram

Our strategy is to study characteristics that serve as proxies for the onset of deconfinement. We exploit an argument based on the Hagedorn limiting temperature concept [7, 13–16]. We compute

the entropy density numerically and impose the criteria $s/T^3 = 4 - 7$ to constrain the range within which the deconfinement transition occurs most rapidly. This leads to the deconfinement bands shown in Fig. 1 for the scenarios without ($eB = 0$) and with ($eB = 0.15$ GeV^2) magnetic field.

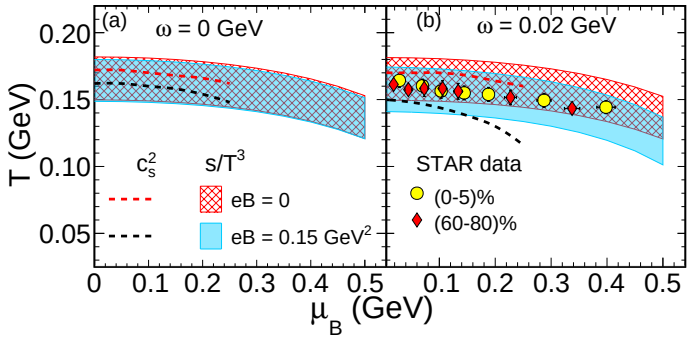

Figure 1: QCD phase diagrams, T vs. μ_B for $eB = 0$ (red band or curve) and $eB = 0.15$ GeV^2 (blue band or curve) and (a) for $\omega = 0$ GeV and (b) for $\omega = 0.02$ GeV. The deconfinement transition zones depicted as (i) bands constrained by $s/T^3 = 4$ (lower edge) and 7 (upper edge) , and (ii) curves obtained from the minima of c_s^2 vs. T.

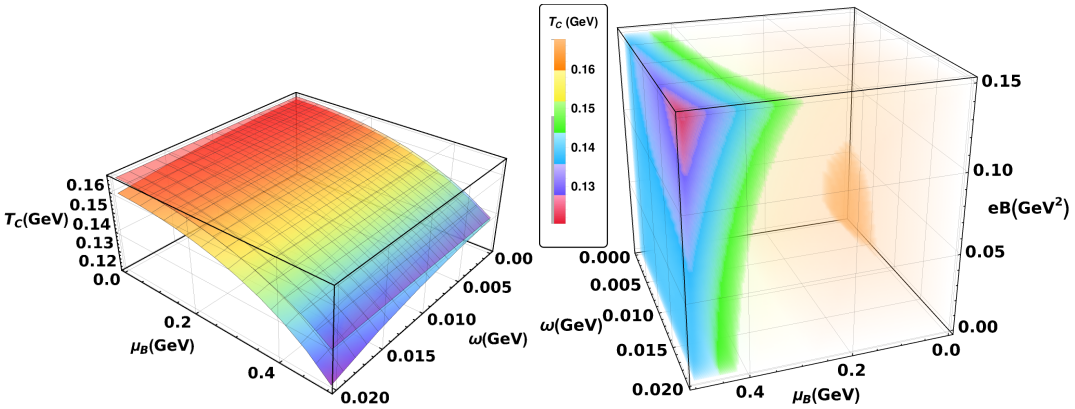

Figure 2: (Top) Deconfinement transition surfaces showing $T_C(\mu_B,\ \omega)$ for $eB = 0$ (upper surface) and $eB = 0.15$ GeV^2 (lower surface). (Bottom) Augmented phase diagram showing $T_C(\mu_B,\ \omega,\ eB)$ as a colour-coded density plot where the T_C-calibrated legend (left) provides reference for the different iso-T_C contour boundaries in the $\mu_B,\ \omega,\ eB$ space. Both plots obtained from rapid rise in entropy density at $s/T^3 = 5.5$.

We observe a successive lowering of the crossover band due to finite magnetic field as ω rise from 0 to 0.02 GeV ($\sim 3 \times 10^{22} s^{-1}$). The dip in T_C is amplified substantially, reaching a nadir nearing 0.1 GeV. At zero magnetic field the effect of rotation with ω rising from 0 to 0.02 GeV is only slight within the range considered here. However, the simultaneous imposition of an external magnetic field over and above the rotation leads to nearly the same drop in the deconfinement temperature at $\omega = 0.02$ GeV as that estimated at extremely large values of $\omega = 0.3$ GeV when there is no magnetic field present at all [7]. This suggests that although the latter (pure, $eB = 0$) rapid rotation scenario might be too high for a typical HIC at deconfinement and freeze-out, a similar (in magnitude) effective lowering of T_C may nevertheless still apply if a strong enough $eB \sim 0.12$ GeV^2 accompanies the more modest but also more plausible $\omega \sim 0.02$ GeV, as we study here. As

the QGP droplet produced in a HIC (particularly those with finite μ_B, ω and eB) evolves from its initial formation to hadronization, the pronounced lowering of T_C may lead to a longer lifetime for the deconfined phase.

In Fig. 1, we have also shown data points for chemical freeze-out [17] for two centrality classes, (0-5)% and (60-80)%. The analyses of peripheral collisions in such studies does not take into account ω and eB. After incorporating all quasi-control parameters (μ_B, ω and eB, all dependent on collision energy and impact parameter or centrality) for freeze-out calculations, instead of a just a $(T - \mu_B)$ curve serving as 'thermometer' and 'baryometer' we can possibly augment them with capabilities of 'magnetometer' and 'anemometer'. The degree of the relative influences of μ_B, ω and eB may be constrained from other simultaneous observables, for example measured polarization [1] to independently constrain ω, etc.

Fig. 2 shows the surface plots (3-D QCD phase diagram) $T_C(\mu_B, \omega)$ for $eB = 0$ and $eB = 0.15$ GeV^2. An even more fine-grained data set is also exhibited in the (4-D QCD phase diagram) $T_C(\mu_B, \omega, eB)$ density plot in Fig. 2.

A dip in the squared speed of sound, c_s^2, reveals the softest point in the equation-of-state and signals a phase transition. Both methods lead to the conclusion that the drop in T_C is strongly enhanced at high μ_B, ω and eB.

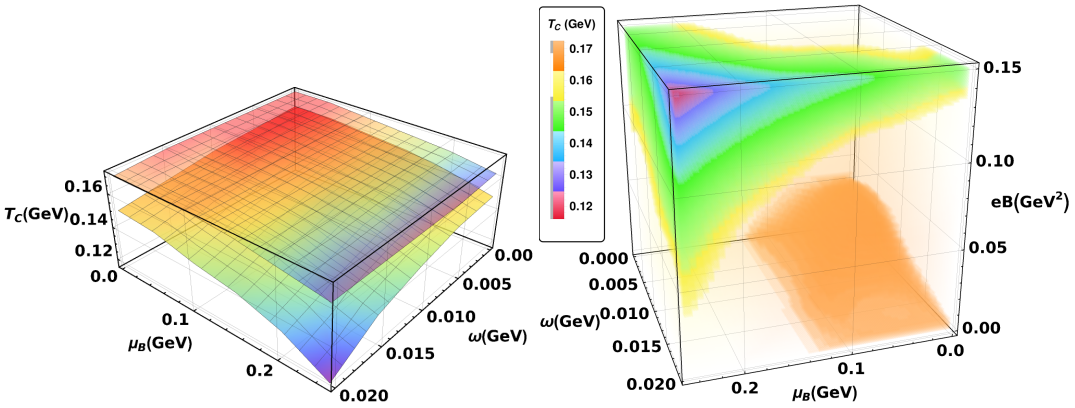

Figure 3: (Top) Deconfinement transition surfaces showing $T_C(\mu_B, \omega)$ for $eB = 0$ (upper surface) and $eB = 0.15$ GeV^2 (lower surface). (Bottom) Augmented phase diagrams showing $T_C(\mu_B, \omega, eB)$, analogous to Fig. 2. Both obtained from the minima of the squared speed of sound.

Figure 3 shows the T_C values obtained from the speed of sound analysis. These results are closely analogous to those shown in Fig. 2.

4. Summary

We expanded the QCD phase structure to accommodate two new phenomenologically important parameters, namely vorticity and magnetic field. The framework of statistical hadronization was implemented to achieve a prediction for the deconfinement temperature T_C as a function of μ_B, ω and eB. We explained a possible strategy to apply this knowledge to trace out freeze-out curves in the higher dimensional phase space and probe HIC fireballs as 'anemometer' and 'magnetometer'. Our work may also shed some light on whether the two approximate transition temperatures (chiral

symmetry breaking/restoration and confinement/deconfinement) stay locked in value or split as we turn on the various parameters to finite values and venture into the (augmented) phase diagram interior. Studying such aspects experimentally in HIC will yield clues about the unsolved issues in QCD such as confinement and shed some new light on the primordial cosmic fluid of the early universe that materialized (hadronized) at the cosmological QCD transition. These are important questions that become even more non-trivial when one adds into the mix vorticity and magnetic fields to create swirling and magnetized complex quantum matter.

References

[1] STAR Collab., "Global hyperon polarization in nuclear collisions," Nature 548, 62–65 (2017)

[2] Yin Jiang, Zi-Wei Lin, and Jinfeng Liao, "Rotating quark-gluon plasma in relativistic heavy-ion collisions," Phys. Rev. C 94, 044910; Erratum Phys. Rev. C 95, 049904 (2017)

[3] Xu-Guang Huang, "Electromagnetic fields and anomalous transports in heavy-ion collisions—a pedagogical review," Rep. Prog. Phys. 79 076302 (2016)

[4] Xingyu Guo, Jinfeng Liao and Enke Wang, Scientific Reports volume 10 (2020)

[5] Kenji Fukushima and Yoshimasa Hidaka, Phys. Rev. Lett. 117, 102301 (2016)

[6] Yizhuang Liu and Ismail Zahed, Phys. Rev. Lett. 120, 032001 (2018)

[7] Yuki Fujimoto, Kenji Fukushima, and Yoshimasa Hidaka, Physics Letters B Volume 816, 136184 (2021)

[8] Yin Jiang and Jinfeng Liao, Phys. Rev. Lett. 117, 192302 (2016)

[9] Gaurav Mukherjee, D. Dutta, D.K. Mishra, Physics Letters B 846, 138228 (2023)

[10] Hao-Lei Chen, K. Fukushima, Xu-Guang Huang, and K. Mameda, Phys. Rev. D 93, 104052 (2016)

[11] Endrődi, G., J. High Energ. Phys. 2013, 23 (2013)

[12] S. Wheaton, J. Cleymans, M. Hauer, "THERMUS—A thermal model package for ROOT"

[13] R. Hagedorn, Nuovo Cim.Suppl. 3 (1965) 147-186

[14] Johann Rafelski, "Melting Hadrons, Boiling Quarks - From Hagedorn Temperature to Ultra-Relativistic Heavy-Ion Collisions at CERN," https://doi.org/10.1007/978-3-319-17545-4

[15] N. Cabibbo, and G. Parisi, Physics Letters B, Volume 59, Issue 1, 13 October 1975

[16] Kenji Fukushima, Physics Letters B, Volume 695, Issues 1–4, 10 January 2011, Pages 387-391

[17] STAR Collaboration, Rom.Rep.Phys. 58 (2006), 049-054